Hadron spectra and elliptic flow for 200 *A* GeV Au + Au collisions from viscous hydrodynamics coupled to a Boltzmann cascade

Huichao Song,[1] Steffen A. Bass,[2] Ulrich Heinz,[3] Tetsufumi Hirano,[1,4] and Chun Shen[3]
[1]*Nuclear Science Division, Lawrence Berkeley National Laboratory, Berkeley, California 94720, USA*
[2]*Department of Physics, Duke University, Durham, North Carolina 27708, USA*
[3]*Department of Physics, The Ohio State University, Columbus, Ohio 43210, USA*
[4]*Department of Physics, The University of Tokyo, Tokyo 113-0033, Japan*
(Received 24 January 2011; revised manuscript received 19 April 2011; published 25 May 2011)

It is shown that the recently developed hybrid code VISHNU, which couples a relativistic viscous fluid dynamical description of the quark-gluon plasma (QGP) with a microscopic Boltzmann cascade for the late hadronic rescattering stage, yields an excellent description of charged and identified hadron spectra and elliptic flow measured in 200 *A* GeV Au + Au collisions at the Relativistic Heavy-Ion Collider (RHIC). Using initial conditions that incorporate event-by-event fluctuations in the initial shape and orientation of the collision fireball and values η/s for the specific shear viscosity of the quark-gluon plasma that were recently extracted from the measured centrality dependence of the eccentricity-scaled, p_T-integrated charged hadron elliptic flow $v_{2,\mathrm{ch}}/\varepsilon$, we obtain universally good agreement between theory and experiment for the p_T spectra and differential elliptic flow $v_2(p_T)$ for both pions and protons at all collision centralities.

DOI: 10.1103/PhysRevC.83.054910 PACS number(s): 12.38.Mh, 25.75.Ld, 24.10.Nz

I. INTRODUCTION

In a recent article [1] we extracted the shear viscosity to entropy density ratio $(\eta/s)_{\mathrm{QGP}}$ of the quark-gluon plasma (QGP) created in heavy-ion collisions at RHIC by comparing experimental data for the eccentricity-scaled elliptic flow v_2/ε with calculations performed with VISHNU [2], a hybrid model that describes the QGP stage of the expansion of the collision fireball macroscopically with viscous hydrodynamics [in which $(\eta/s)_{\mathrm{QGP}}$ enters as an input parameter] but switches to a microscopic description in the late hadronic phase where we solve the Boltzmann equation with UrQMD [3]. An important step in this analysis was to ensure that, as we compared theoretical curves for different $(\eta/s)_{\mathrm{QGP}}$ values with the experimental data in order to find the value preferred by nature, we maintained a good description of the total charged hadron multiplicity and the hadron transverse momentum spectra as a function of collision centrality. That this was indeed achieved was announced in Ref. [1] and will be documented in this companion article. We then proceed to demonstrate that, with the QGP shear viscosity extracted in [1], VISHNU provides a good description of all single-particle aspects of soft hadron production in 200 *A* GeV Au + Au collisions for which accurate measurements exist, over the entire range of collision centralities.

II. METHODOLOGY

The various components of the viscous hydrodynamics + Boltzmann hybrid code VISHNU have been described in Ref. [2] (see also [3–5]) to which we refer the reader interested in technical details. For the QGP fluid we approximate η/s in the temperature range $T_c < T \lesssim 2T_c$ by a constant [6]. We switch from a hydrodynamic description of the QGP to the microscopic hadronic rescattering code UrQMD at temperature $T_{\mathrm{sw}} = 165$ MeV, adjusted to reproduce the chemical freeze-out temperature measured in RHIC collisions [7]; as shown in [2], this is at the same time the *highest* T for which we have a valid microscopic description and the *lowest* T for which the macroscopic hydrodynamic approach can be trusted.

As shown in Refs. [1,8], the QGP shear viscosity $(\eta/s)_{\mathrm{QGP}}$ extracted from the experimentally measured elliptic flow depends on the initial fireball eccentricity $\varepsilon_{\mathrm{part}} = \frac{\langle y^2 - x^2\rangle}{\langle y^2 + x^2\rangle}$ where x and y label the coordinates along the short and long major axes of the fireball in the plane transverse to the beam direction. (This definition of x, together with the beam direction z, define the "participant plane", reflected in the subscript.) With presently available tools this initial eccentricity cannot be directly measured, and theoretically we have limited control over it. We here use initial entropy density profiles from two popular geometric models for the initial particle production in high-energy heavy-ion collisions, the Monte Carlo Glauber model (MC-Glauber [9]), in a version [10] that uses finite size nucleons, and the Monte Carlo fKLN (MC-KLN) model [10–12]. These models give initial eccentricities that differ (depending on centrality) by up to 25% which we hope to cover the physically reasonable range of uncertainty. We showed in [1] that this uncertainty in the initial eccentricity completely dominates the present error range in the phenomenological extraction of $(\eta/s)_{\mathrm{QGP}}$, and that future improvements in the accuracy of the experimentally extracted value of $(\eta/s)_{\mathrm{QGP}}$ cannot be achieved without obtaining better (experimental and/or theoretical) control over the initial fireball eccentricity.

Due to the finite number of nucleons colliding with each other in a heavy-ion collision, the initial eccentricity of the density of secondary particles produced in these collisions fluctuates from event to event, as does the orientation of its major and minor axes relative to the reaction plane [13] (defined by the directions of the impact parameter and the beam). To account for these event-by-event fluctuations on average, we use a Monte Carlo sampling procedure to generate from the

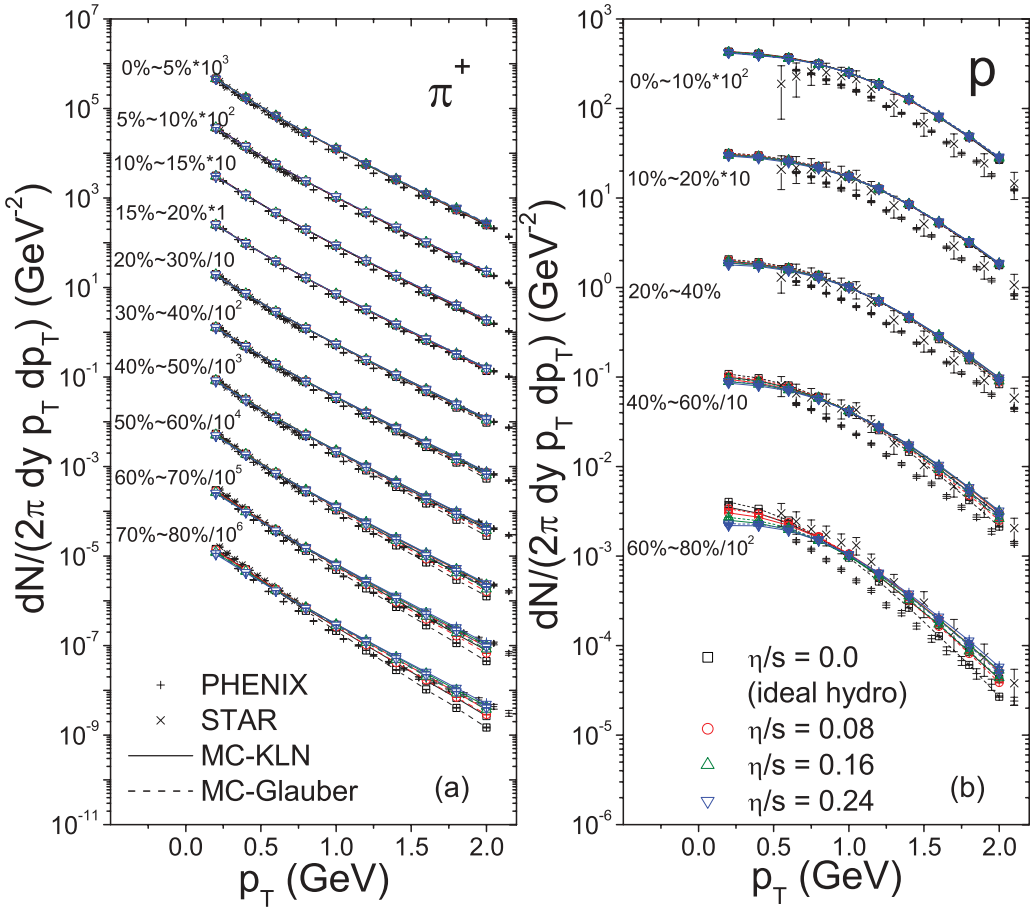

FIG. 1. (Color online) p_T spectra of pions (left) and protons (right) for 200 A GeV Au + Au collisions of different centralities as indicated. Data from the STAR (×, [15–17]) and PHENIX (+, [18]) experiments are compared with VISHNU calculations using MC-Glauber (dashed lines) or MC-KLN initial conditions (solid lines) and different values η/s for the QGP shear viscosity as indicated. Different η/s values are associated with different starting times τ_0 for the hydrodynamic evolution as discussed in the text. The STAR and PHENIX proton data shown in the right column are feeddown corrected by removing protons from weak hyperon decays [15,18]. Where necessary, PHENIX yields from neighboring narrower centrality bins were averaged to obtain data in the wider centrality bins used by the STAR Collaboration.

Glauber and fKLN models a large number of initial entropy density distributions whose shape and orientation fluctuate from event to event, recenter, and rotate each distribution around the beam direction such that its short major axis x aligns with the direction of the impact parameter $\boldsymbol{b}$, sort them into centrality bins by $N_{\rm part}$ (the number of wounded nucleons), and then superimpose the distributions to obtain a smooth average density that has the correct average eccentricity for collisions in this centrality class.[1] The elliptic flow resulting from the VISHNU evolution of this initial profile is interpreted as the event-average $\langle v_2 \rangle$ for the selected centrality class.

The ensemble-averaged initial entropy density is normalized such that, after evolution with VISHNU, it reproduces the measured final charged hadron rapidity density $dN_{\rm ch}/dy$ in the most central collisions [17]; due to viscous entropy production this is an iterative process, requiring two or three iterations. After normalization in central collisions, the centrality dependence of the initial entropy production is taken directly from the model (MC-Glauber or MC-KLN); for the MC-Glauber model we follow [10,14] and assume a two-component (soft + hard) model with a small hard fraction ($\delta = 0.14$ [10]) for the entropy production. In [10] this fraction was fixed within a hydro + Boltzmann hybrid approach using ideal fluid dynamics for the QGP; taking the same fraction in our viscous hydro + Boltzmann code ignores the centrality dependence of viscous heating. We have checked that its effects on the centrality dependence of the final $dN_{\rm ch}/dy$ are negligible relative to experimental uncertainties.

[1]Strictly speaking, this procedure yields $\bar{\varepsilon}_{\rm part} \equiv \frac{\langle y^2 - x^2 \rangle_{\bar{s}}}{\langle y^2 + x^2 \rangle_{\bar{s}}}$ where $\langle \cdots \rangle_{\bar{s}}$ denotes the expectation value taken with the averaged entropy density obtained by superimposing many recentered and rotated Monte Carlo events; this is not identical with, but numerically very close to the ensemble-averaged participant eccentricity $\langle \varepsilon_{\rm part} \rangle$ where for each event $\varepsilon_{\rm part}$ is computed as the analogous expectation value taken with the entropy density of that event.

III. RESULTS: COMPARISON OF SPECTRA AND v_2 TO DATA

Let us now begin discussing our results. All experimental data and theoretical calculations are for 200 A GeV Au + Au collisions. Figure 1 shows pion and proton transverse

momentum spectra from the STAR [15–17] and PHENIX [18] Collaborations for the whole range of collision centralities, separated by multiplicative factors of 10 for clarity. The lines show VISHNU calculations for different values of $(\eta/s)_{\rm QGP}$ in the QGP phase, using either MC-KLN (solid) or MC-Glauber (dashed) initial conditions. When changing $(\eta/s)_{\rm QGP}$ we have to (i) renormalize the initial entropy density profiles by a (b-independent) constant factor to account for the change in viscous entropy production, and (ii) adjust τ_0 to account for the additional radial acceleration caused by the transverse shear pressure gradients. The latter increase with $(\eta/s)_{\rm QGP}$, leading to more radial flow and flatter p_T spectra unless we compensate by increasing the starting time for the hydrodynamic evolution accordingly. The curves shown in Fig. 1 correspond to the following parameter pairs $(\eta/s,\ c\tau_0)$: (0, 0.4 fm), (0.08, 0.6 fm), (0.16, 0.9 fm), and (0.24, 1.2 fm). We stop at $\eta/s = 0.24$ since we will see that larger QGP shear viscosities are excluded by the elliptic flow data.

Except for very peripheral collisions, the different lines in Fig. 1 overlap almost perfectly and thus are hard to distinguish optically. This is intentional since it shows the approximate equivalence of the different parameter pairs as far as the quality of the theoretical description of the measured p_T spectra goes. Differences between theory and data are generally less than between data sets from the different experiments. We note that the theoretical proton spectra are uniformly about 50% larger than the PHENIX data but agree nicely with their slope; their normalization agrees somewhat better with the STAR data. Due to limited event statistics, VISHNU does not include protons from weak decays; in Fig. 1(b) we therefore compare with experimental data that have been corrected to eliminate feeddown protons. However, the feeddown correction methods used by PHENIX and STAR differ [15,18], and systematic uncertainties arising from the feeddown correction are large. Keeping the differences between the experimental data sets in mind, VISHNU provides a very acceptable compromise description. We do note in passing that in the most peripheral bins a viscous treatment of the QGP appears to work better than treating it as an ideal fluid; assuming zero viscosity for the QGP gives too little radial flow and results in p_T spectra for both pions and protons that are slightly too steep.

Figure 2 shows the differential elliptic flow $v_2(p_T)$ for charged hadrons from Au + Au collisions at different centralities. Experimental data from the STAR Collaboration obtained with the event-plane method [19] are compared with

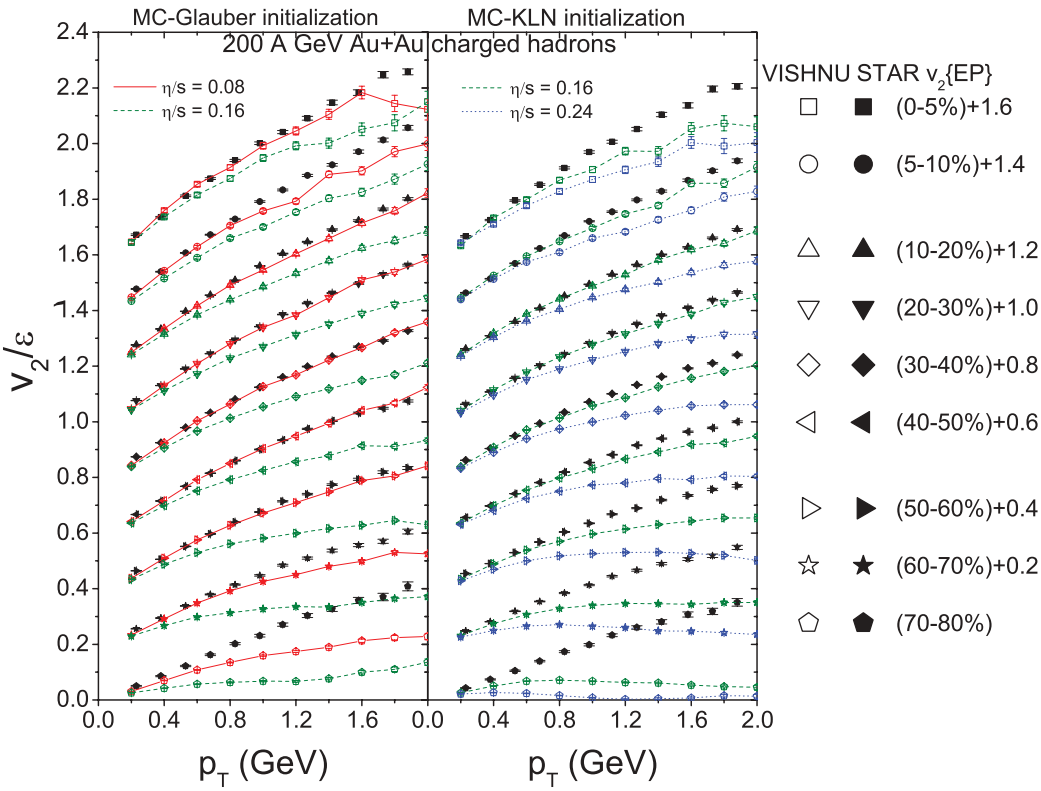

FIG. 2. (Color online) Eccentricity-scaled elliptic flow v_2/ε as function of p_T for charged hadrons from 200 A GeV Au + Au collisions at different centralities. The experimental data (solid symbols) are $v_2\{\rm EP\}$ measurements from the STAR experiment [19], scaled by $\langle\varepsilon_{\rm part}^{\alpha}\rangle^{1/\alpha}$ from the Monte Carlo Glauber model (left column) and the MC-KLN model (right column), respectively. α depends on the event-plane resolution R and varies from one centrality bin to the next (see Table I). Dashed and solid lines with open symbols are results from VISHNU for two different values of $(\eta/s)_{\rm QGP}$ (0.08 and 0.16 for the MC-Glauber calculations, 0.16 and 0.24 for the MC-KLN calculations). The theoretical lines show the ratio $\langle v_2\rangle/\bar{\varepsilon}_{\rm part}$ where $\langle\cdots\rangle$ denotes an average over events, and $\bar{\varepsilon}_{\rm part}$ is the eccentricity of the smooth average initial entropy density. Different symbols denote different collision centralities as indicated.

TABLE I. Mean ($\bar{\varepsilon}_{\rm part} \approx \langle \varepsilon_{\rm part} \rangle$) and rms ($\varepsilon\{2\} = \sqrt{\langle \varepsilon_{\rm part}^2 \rangle}$) participant eccentricities, as well as $\langle \varepsilon_{\rm part}^{\alpha} \rangle^{1/\alpha}$, with α computed from the event-plane resolution R as described in [21,28], for the STAR [19] and PHENIX [25] Au + Au experiments at different collision centralities. For centralities between 10% and 50%, PHENIX [25] published data in 5% centrality increments. For the purpose of comparing the PHENIX and STAR data we combined the PHENIX data [25] from neighboring centrality bins, by averaging the event-plane resolutions R and the exponents α corresponding to the two sub-bins when computing $\langle \varepsilon_{\rm part}^{\alpha} \rangle^{1/\alpha}$ for the larger combined bin. All eccentricities are calculated with the entropy density as weight.

Centrality	Model	$\bar{\varepsilon}_{\rm part}$	$\sqrt{\langle \varepsilon_{\rm part}^2 \rangle}$	STAR			PHENIX		
				R [19]	α [21,28]	$\langle \varepsilon_{\rm part}^{\alpha} \rangle^{1/\alpha}$	R [25]	α [21,28]	$\langle \varepsilon_{\rm part}^{\alpha} \rangle^{1/\alpha}$
0%–5%	MC-Glauber	0.089	0.101	0.61	1.52	0.095	0.51	1.66	0.097
	MC-KLN	0.097	0.109			0.103			0.105
5%–10%	MC-Glauber	0.139	0.153	0.735	1.31	0.144	0.63	1.49	0.146
	MC-KLN	0.172	0.183			0.175			0.178
10%–20%	MC-Glauber	0.215	0.230	0.816	1.18	0.218	0.720	1.33	0.220
	MC-KLN	0.265	0.277			0.267			0.269
20%–30%	MC-Glauber	0.299	0.311	0.843	1.14	0.298	0.743	1.30	0.301
	MC-KLN	0.360	0.372			0.362			0.364
30%–40%	MC-Glauber	0.361	0.378	0.825	1.16	0.364	0.704	1.36	0.367
	MC-KLN	0.434	0.447			0.436			0.439
40%–50%	MC-Glauber	0.414	0.433	0.771	1.25	0.419	0.617	1.50	0.424
	MC-KLN	0.493	0.509			0.497			0.501
50%–60%	MC-Glauber	0.458	0.481	0.677	1.41	0.468	0.489	1.69	0.475
	MC-KLN	0.541	0.561			0.549			0.555
60%–70%	MC-Glauber	0.497	0.523	0.549	1.61	0.513	–	–	–
	MC-KLN	0.581	0.606			0.597			
70%–80%	MC-Glauber	0.528	0.560	0.412	1.78	0.554	–	–	–
	MC-KLN	0.621	0.650			0.645			

VISHNU calculations for different QGP shear viscosities. $v_2\{\rm EP\}$ receives positive contributions from event-by-event flow fluctuations and nonflow effects [20]. The latter can be minimized by trying to decorrelate the determination of the event plane from the measurement of v_2, for example, by employing a large rapidity gap between these measurements. Fluctuation effects cannot be eliminated from the measurement, but both nonflow and fluctuations can be corrected for [21]. In [1] we used such corrected data to extract $(\eta/s)_{\rm QGP}$; in Fig. 2 we show the uncorrected $v_2\{\rm EP\}$ data directly as measured. To account for the fluctuation contribution we normalize them by $\langle \varepsilon_{\rm part}^{\alpha} \rangle^{1/\alpha}$ [21,22] where the exponent α depends on the experimental event-plane resolution R and on details of the v_2 extraction method [21]. In Table I we have summarized for each centrality bin shown in Figs. 2–4 the event-plane resolution factors R for the STAR and PHENIX experiments, the corresponding α values obtained from the procedure described in Ref. [21], as well as the corresponding values for $\langle \varepsilon_{\rm part} \rangle$, $\langle \varepsilon_{\rm part}^2 \rangle^{1/2}$, and $\langle \varepsilon_{\rm part}^{\alpha} \rangle^{1/\alpha}$. In Fig. 2 we compare the experimental ratio $v_2\{\rm EP\}/\langle \varepsilon_{\rm part}^{\alpha} \rangle^{1/\alpha}$ with the theoretically calculated ratio $\langle v_2 \rangle/\bar{\varepsilon}_{\rm part}$. This is the correct comparison if $v_2 \sim \varepsilon_{\rm part}$ event by event, as suggested by hydrodynamic simulations [23] (see, however, [24]).

Figure 2 demonstrates excellent agreement between VISHNU and the experimental data over the entire range of centralities except for the two most peripheral bins, if we use $(\eta/s)_{\rm QGP} = 0.08$ for MC-Glauber (left column) and $(\eta/s)_{\rm QGP} = 0.16$ for MC-KLN initial conditions (right column).[2] These values are a little smaller than, but consistent with the corresponding values $(\eta/s)_{\rm QGP} \simeq 0.1$ for MC-Glauber and $(\eta/s)_{\rm QGP} \simeq 0.2$ for MC-KLN that were extracted in [1] from the p_T-integrated, nonflow and fluctuation corrected charged hadron v_2. Small nonflow effects in the $v_2\{\rm EP\}$ data shown here, shifting them slightly upward, may account for this difference.

[2]Figure 2 also shows that in both cases the agreement is destroyed when increasing $(\eta/s)_{\rm QGP}$ by $\frac{1}{4\pi} = 0.08$.

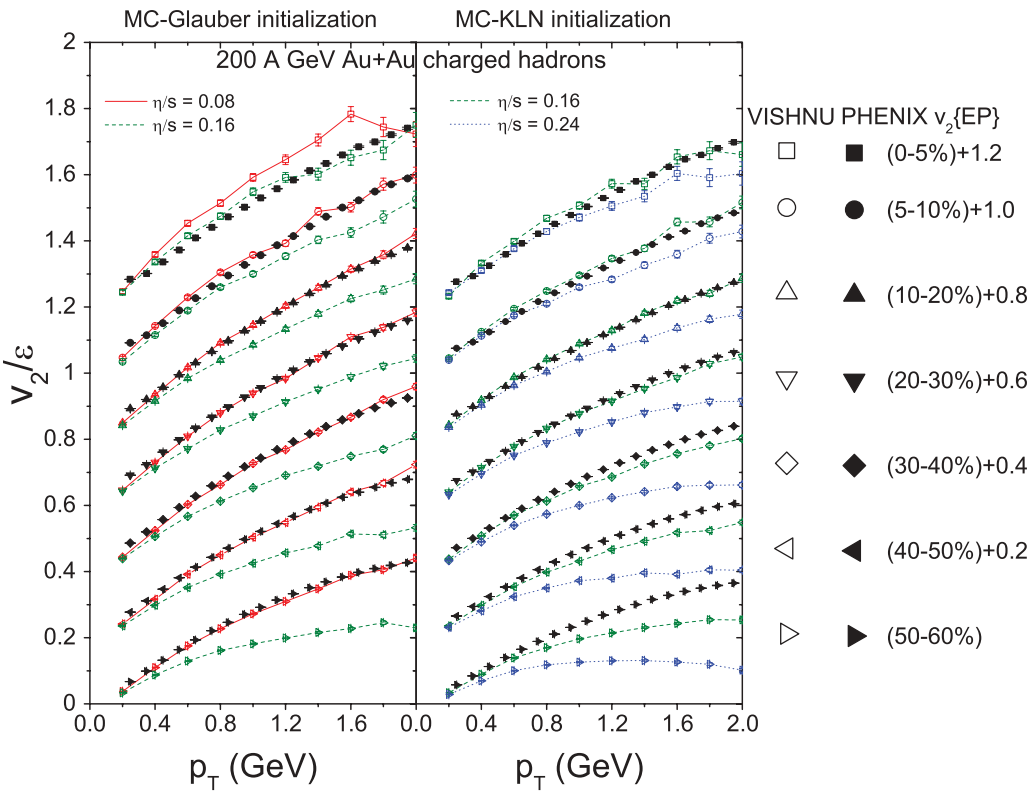

FIG. 3. (Color online) Same as Fig. 2, but with $v_2\{\mathrm{EP}\}$ data from the PHENIX Collaboration [25] instead of STAR data. See Table I for the effective eccentricities $\langle \varepsilon_{\mathrm{part}}^{\alpha} \rangle^{1/\alpha}$ used for each centrality bin.

To check this possibility we show in Fig. 3 the same comparison with PHENIX data for $v_2\{\mathrm{EP}\}$ [25] where the event plane was determined with counters several units of rapidity away from the central region where v_2 was measured. The PHENIX data should therefore be less affected by nonflow effects than the STAR data. For centralities $>10\%$ the agreement between VISHNU calculations and the PHENIX data is equally good as in Fig. 2 for the STAR data, with the same values for $(\eta/s)_{\mathrm{QGP}}$. In the two most central bins, 5%–10% and 0%–5%, respectively, the agreement deteriorates significantly, with the PHENIX data pointing counterintuitively to *larger* $(\eta/s)_{\mathrm{QGP}}$ values for central collisions than in the other centrality bins. Figure 4 shows that this results from a disagreement between the two data sets in near-central collisions: while the two data sets overlap excellently for centralities $>20\%$, they increasingly diverge at small centralities, with a 30% difference between STAR an PHENIX in the 0%–5% centrality bin. It has been pointed out that the excess of the STAR over the PHENIX data is uniform in p_T and could be explained by a 2% shift in the centrality definitions between the experiments [26]. Where such a shift could arise from and which of the two definitions needs to be corrected is presently under study [27]. We conclude from Figs. 2–4 that (i) nonflow effects seem to be similar and likely small in both STAR and PHENIX $v_2\{\mathrm{EP}\}$ data for centralities between 20% and 60%, (ii) if the STAR centrality definition is correct we have excellent agreement between VISHNU and the experimental charged hadron elliptic flow $v_2(p_T)$ at all centralities, with $(\eta/s)_{\mathrm{QGP}} = 0.08$ for MC-Glauber and $(\eta/s)_{\mathrm{QGP}} = 0.16$ for MC-KLN initial conditions, and (iii) if the PHENIX centrality definition is correct, this uniform agreement is broken in the most central collisions for which the PHENIX data appear to require larger effective $(\eta/s)_{\mathrm{QGP}}$ values than at larger centralities.

Figure 5 demonstrates that the agreement of VISHNU using the phenomenologically extracted $(\eta/s)_{\mathrm{QGP}}$ values from Ref. [1] with the measured differential elliptic flow carries over from all charged hadrons to identified pions and protons. Data for protons that have sufficient statistical precision to discriminate between different $(\eta/s)_{\mathrm{QGP}}$ values exist only for the midcentrality range 20%–50%. In very peripheral collisions ($>60\%$ centrality) VISHNU has similar problems with the pion $v_2(p_T)$ as we saw in Figs. 2 and 3 for all charged hadrons. (We comment on this discrepancy in the discussion in Sec. IV.) In the midcentrality range Fig. 5 shows excellent agreement between VISHNU with $(\eta/s)_{\mathrm{QGP}} = 0.08$ for MC-Glauber and $(\eta/s)_{\mathrm{QGP}} = 0.16$ for MC-KLN initial conditions and the experimental data, in each of the three, respectively, four centrality bins shown. The pion elliptic flow data in the left column reveal that for both MC-Glauber and MC-KLN initial conditions this agreement breaks down if $(\eta/s)_{\mathrm{QGP}}$ is increased by $\frac{1}{4\pi} = 0.08$ above the preferred value. For protons the calculation of $v_2(p_T)$ is numerically costly (the elliptic flow signal and the number of protons per event are both small), and we have therefore not done any calculations for other than the preferred $(\eta/s)_{\mathrm{QGP}}$ values. However, the

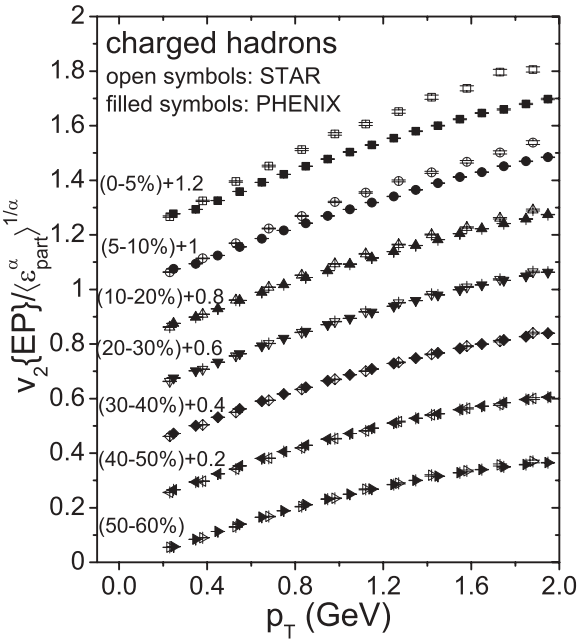

FIG. 4. Comparison of the STAR [19] and PHENIX $v_2\{EP\}$ data [25] used in Figs. 2 and 3. Both data sets are scaled by the effective eccentricity $\varepsilon \equiv \langle \varepsilon_{\rm part}^{\alpha} \rangle^{1/\alpha}$, where α depends on the event-plane resolution R [21] and thus varies with centrality and from experiment to experiment (see Table I).

proton data for these bins are precise enough that they would again reject $(\eta/s)_{\rm QGP}$ values that differed by more than $1/4\pi$ from the values shown.

IV. DISCUSSION

The comparisons between theory and data discussed above prove that we can extract the QGP shear viscosity from the centrality dependence of the p_T-*integrated* v_2 for charged hadrons and then use this value to obtain a very good overall description of the p_T-*differential* v_2. This works not only for the sum of all charged hadrons, but also for individual identified hadronic species, and it carries over from v_2 to their p_T spectra which are nicely described over the entire range of collision centralities, except perhaps the most peripheral collisions.

We do not recommend to try to extract $(\eta/s)_{\rm QGP}$ directly from the p_T-differential elliptic flow for the following reasons. The main effect of shear viscosity that we exploit when extracting it from experiment is that it inhibits the hydrodynamic conversion of spatially anisotropic pressure gradients within the collision fireball into momentum anisotropies. As emphasized by Ollitrault [29], Heinz [30], and recently by Teaney [31], the p_T-integrated elliptic flow[3] of the sum of all hadrons is the observable that has the most direct relationship with the hydrodynamically generated total momentum anisotropy.[4] Hence it is *the total charged hadron* v_2 that is controlled by η/s. How the hydrodynamically generated total momentum anisotropy is distributed among the different hadron species and in p_T depends on the chemical composition and p_T distributions of the hadrons [32].

The correct theoretical description of the differential elliptic flow $v_2(p_T)$ of individual identified hadron species thus depends on the accurate reproduction of their yields and p_T spectra which show much stronger sensitivities to details of the hydrodynamic simulation (such as initial conditions and shape of the initial density profiles) than the total momentum anisotropy itself. For example, in a purely hydrodynamic approach with Cooper-Frye freeze-out, even at extremely high collision energies where the total momentum anisotropy has time to fully saturate before freeze-out, lower freeze-out temperatures will lead to more radial flow; this affects the slope of the single-particle spectra, causing a concomitant change in the slope of $v_2(p_T)$ which is solely controlled by the fact that, after integration over p_T, the same total charged hadron elliptic flow must be reproduced as for a higher freeze-out temperature. In a hybrid approach such as ours, the Cooper-Frye procedure used to convert the hydrodynamic output into particle distributions involves a so-called "δf correction" [33] describing the deviation from local equilibrium on the conversion hypersurface; its form is presently not precisely known [34,35]. For a given total charged hadron v_2, different parametrizations for δf lead to different shapes of identified hadron spectra and $v_2(p_T)$. Bulk viscosity has very little effect on the total momentum anisotropy (and thus on the total charged hadron v_2) but affects the radial flow and hence the slopes of p_T spectra and $v_2(p_T)$ [35,36]. These interdependencies between the hadron p_T spectra and their p_T-dependent elliptic flow make it hazardous to extract $(\eta/s)_{\rm QGP}$ from $v_2(p_T)$. With such an approach it is rather difficult to arrive at a uniformly good description of all soft hadron characteristics, and one easily ends up with different $(\eta/s)_{\rm QGP}$ values extracted from the elliptic flow of different hadron species or from collisions at different centralities.

When using the p_T-integrated charged particle elliptic flow to extract $(\eta/s)_{\rm QGP}$ one must, however, pay attention to the fact that the measured elliptic flow fluctuates from event to event and may be contaminated by nonflow contributions. This was emphasized in Ref. [1] where we therefore used elliptic flow data that had been corrected for nonflow effects and event-by-event fluctuations. In the remainder of this article we elaborate on how the p_T-integrated charged hadron elliptic flow $\langle v_2 \rangle$ from the dynamical model VISHNU, calculated with the $(\eta/s)_{\rm QGP}$ values extracted in [1], compares directly with various experimental measurements that have not been corrected for fluctuation and nonflow effects. The trends exposed in this comparison provide useful insights.

[3]More precisely: the p_T^2-weighted elliptic flow $A_2 \equiv \frac{\langle p_x^2 - p_y^2 \rangle}{\langle p_x^2 + p_y^2 \rangle}$, rather than $v_2 = \langle \cos(2\phi_p) \rangle \equiv \langle \frac{p_x^2 - p_y^2}{p_x^2 + p_y^2} \rangle$.

[4]Replacing "all hadrons" by "all charged hadrons" is fine because of approximate symmetry between positive, negative, and uncharged hadrons in ultrarelativistic collisions which generate almost baryon-free fireballs.

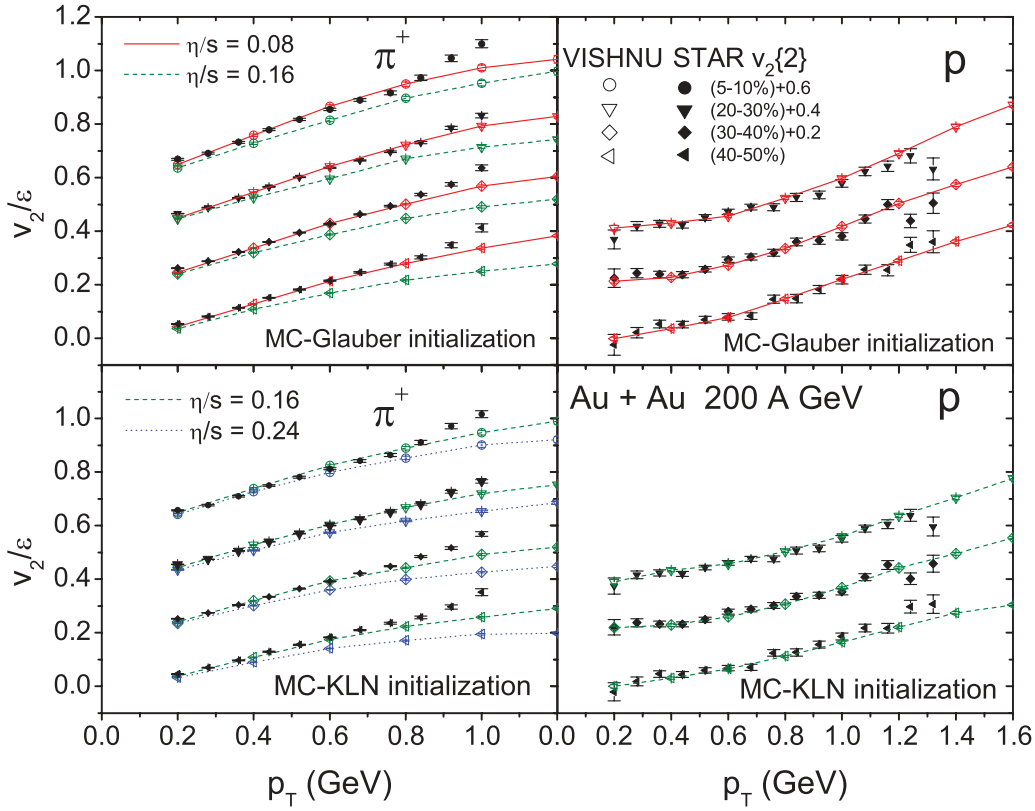

FIG. 5. (Color online) Same as Fig. 2 but for identified pions (left column) and protons (right column). Solid symbols denote measurements of $v_2\{2\}/\langle\varepsilon_{\rm part}^2\rangle^{1/2}$ from the STAR experiment [19], solid and dashed lines with open symbols show $\langle v_2\rangle/\bar{\varepsilon}_{\rm part}$ from VISHNU calculations with $(\eta/s)_{\rm QGP} = 0.08$ and 0.16, respectively, using MC-Glauber (top row) and MC-KLN (bottom row) initial conditions. Different symbols denote different collision centralities as indicated.

Without the ability of doing event-by-event hydrodynamic simulations [24,37,38], we can at this moment account for event-by-event fluctuations of the initial fireball density distribution only on average, in one of two ways: Either we recenter and rotate each Monte Carlo event, in order to align their major and minor axes, before averaging the density distributions [this produces an average density profile $\bar{s}_{\rm part}$ in the "participant plane", characterized by its average eccentricity $\bar{\varepsilon}_{\rm part} \approx \langle\varepsilon_{\rm part}\rangle$ (see footnote), or we superimpose the densities without recentering and rotating [producing a smooth average density profile $\bar{s}_{\rm RP}$ in the "reaction plane", with "standard" eccentricity $\varepsilon_{\rm s} = \frac{\langle y^2-x^2\rangle}{\langle y^2+x^2\rangle}$ where (in contrast to footnote) the expectation values in numerator and denominator are taken with $\bar{s}_{\rm RP}$]. Both of these methods incorporate (in different ways) the effect of event-by-event fluctuations of the shape and orientation of the collision fireball on the average initial eccentricity, but do not dynamically propagate event-by-event fluctuations of the value of this eccentricity. As a result, the hydrodynamic evolution produces a nonfluctuating elliptic flow, and while the UrQMD afterburner produces event-by-event v_2 fluctuations, they are only due to finite number statistics and not related to event-by-event fluctuations of the initial eccentricity ε.

Various experimental techniques measure different varieties of v_2 which are affected in different ways by event-by-event flow fluctuations (driven by event-by-event variations of the initial eccentricity) and nonflow effects. Hydrodynamic simulations with smooth (nonfluctuating) initial conditions indicate a linear relationship $v_2 \propto \varepsilon$ for not too large eccentricity [23].[5] If $v_2 \propto \varepsilon$, the probability distribution of the final v_2 is directly related to that of the initial ε. For example, a measurement of $\sqrt{\langle v_2^2\rangle}$ would yield values that are proportional to $\sqrt{\langle\varepsilon^2\rangle}$, with the same proportionality constant as between $\langle v_2\rangle$ and $\langle\varepsilon\rangle$ [39]. Unfortunately, quantities like $\varepsilon_{\rm part}\{2\} = \langle\varepsilon_{\rm part}^2\rangle^{1/2}$ and $\varepsilon_{\rm part}\{4\} = [2\langle\varepsilon_{\rm part}^2\rangle^2 - \langle\varepsilon_{\rm part}^4\rangle]^{1/4}$ that control the fluctuation contributions to $v_2\{2\}$ and $v_2\{4\}$ [20,21], have a different centrality dependence than the average eccentricities $\bar{\varepsilon}_{\rm part}$ and $\varepsilon_{\rm s}$ that characterize our hydrodynamic initial conditions. For this reason it has been suggested in [39] to make comparisons between theory and experiment only with appropriately normalized elliptic flows. In the absence of nonflow contributions and for a linear mapping between ε

[5]Event-by-event hydrodynamic simulations with fluctuating initial conditions show that flow anisotropy and eccentricity coefficients of different harmonic order do not completely decouple from each other [24,38], and in both single-shot and event-by-event hydrodynamic simulations we have seen evidence [24] that in very central collisions the (small) final elliptic flow is affected by several harmonic eccentricity coefficients in the initial state (which, although all small, are of similar order of magnitude), resulting in a nonlinear dependence of v_2 on ε for small v_2.

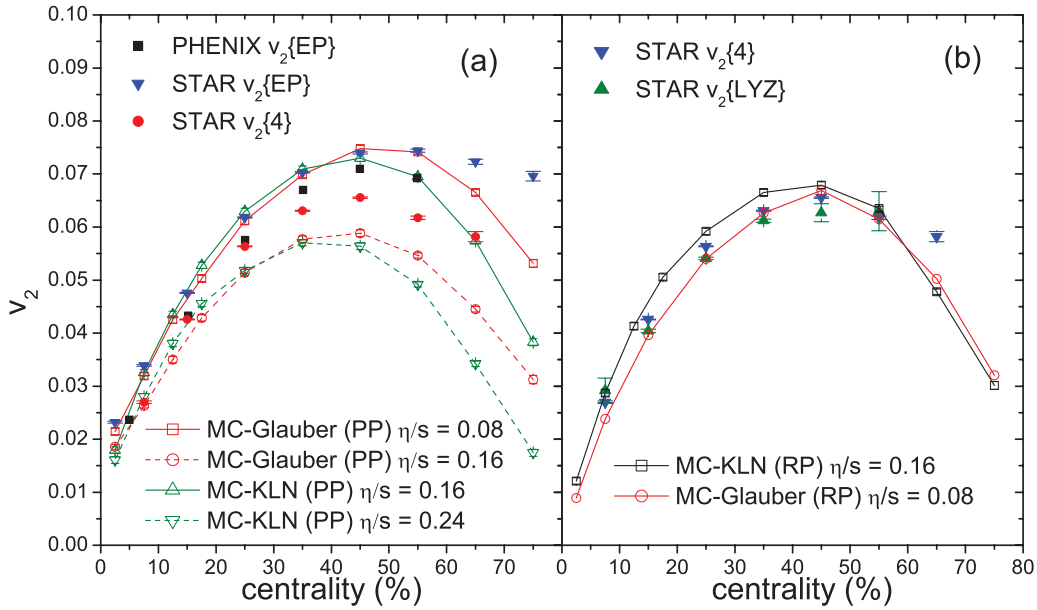

FIG. 6. (Color online) Integrated charged hadron elliptic flow as a function of collision centrality from the PHENIX [44] and STAR [19,43] experiments are compared with VISHNU calculations using participant plane (PP) averaged (a) and reaction plane (RP) averaged (b) initial conditions from the MC-KLN and MC-Glauber models and $(\eta/s)_{\rm QGP}$ values as indicated. In the STAR data and the calculations v_2 was integrated over the range 0.15 GeV/c < p_T < 2GeV/c; the PHENIX data were integrated over 0.2GeV/c < p_T < 8GeV/c.

and v_2 in each event, one has $\langle v_2\rangle/\langle\varepsilon_{\rm part}\rangle = v_2\{2\}/\varepsilon_{\rm part}\{2\} = v_2\{4\}/\varepsilon_{\rm part}\{4\}$ where the first ratio can be calculated in a single-shot hydrodynamic evolution of an average initial profile, whereas the other two ratios can be measured if the initial eccentricity and its fluctuations are known from a model.

For Gaussian fluctuations $P(\varepsilon_{\rm part})\sim\exp[-\frac{(\varepsilon_{\rm part}-\bar{\varepsilon})^2}{2\sigma^2}]$ it is easy to show [13] that $\varepsilon_{\rm part}\{2\} = (\langle\varepsilon_{\rm part}\rangle^2+\sigma^2)^{1/2}$ receives a positive contribution from fluctuations, whereas $\varepsilon_{\rm part}\{4\} = (\langle\varepsilon_{\rm part}\rangle^4 - 2\sigma^2\langle\varepsilon_{\rm part}\rangle^2 - \sigma^4)^{1/4}$ is reduced relative to $\langle\varepsilon_{\rm part}\rangle$. (In fact, we can write in general $\varepsilon_{\rm part}\{4\} = [\langle\varepsilon^2_{\rm part}\rangle^2-(\langle\varepsilon^4_{\rm part}\rangle - \langle\varepsilon^2_{\rm part}\rangle^2)]^{1/4}$ in terms of the difference between two positive definite quantities which, for non-Gaussian distributions, can become negative, in which case $\varepsilon_{\rm part}\{4\}$ is not defined.) It has been observed in [40] that, for models where $\varepsilon_{\rm part}$ shows Bessel-Gaussian fluctuations [40,41], $\varepsilon_{\rm part}\{4\}$ agrees exactly with the reaction plane eccentricity $\langle\varepsilon_{\rm RP}\rangle \approx \varepsilon_{\rm s}$, and in [21] that $v_2\{4\}$ is insensitive to two-particle nonflow contributions. For these reasons, the authors of [42] used hybrid model simulations with reaction-plane averaged initial conditions for direct comparison with RHIC Au + Au and recent LHC Pb + Pb data [43]. The validity of the assumption of (Bessel)-Gaussian eccentricity and flow fluctuations has been challenged in [22] but was recently validaded for the MC-Glauber and MC-KLN models for Au + Au collisions at centralities of up to about 40% [24]; for more peripheral collisions, the assumption breaks down. We here compare results obtained from both participant-plane and reaction-plane averaged initial conditions with p_T-integrated $v_2\{4\}$ data.

In Fig. 6 we compare VISHNU results with STAR and PHENIX data for the integrated charged hadron elliptic flow as function of collision centrality. The STAR and PHENIX data are integrated over slightly different p_T ranges; correcting the PHENIX data for the somewhat smaller lower p_T cutoff used by STAR and in the calculations would move them slightly down. In the absence of nonflow contributions and the limit of small fluctuations, $v_2\{\rm EP\} \approx \sqrt{\langle v_2\rangle^2+\sigma_v^2}$ and $v_2\{4\} \approx \sqrt{\langle v_2\rangle^2-\sigma_v^2}$. Nonflow effects would push $v_2\{\rm EP\}$ further up but leave $v_2\{4\}$ unchanged. Calculations with reaction-plane averaged initial conditions of eccentricity $\bar{\varepsilon}_{\rm part}$ [Fig. 6(a)] should thus fall between $v_2\{\rm EP\}$ and $v_2\{4\}$, perhaps a bit closer to $v_2\{4\}$ if the $v_2\{\rm EP\}$ data are affected by nonflow. The STAR $v_2\{\rm EP\}$ data lie above those of PHENIX, consistent with the expectation that the PHENIX data should have less nonflow contributions (if any at all), but some of the difference between the data set (especially at small centralities) may also originate from a shift in the centrality definition [26]. Except for the most peripheral centralities, our calculations lie above the PHENIX and roughly on the STAR $v_2\{\rm EP\}$ data and overpredict the STAR $v_2\{4\}$ data. This indicates that the chosen $(\eta/s)_{\rm QGP}$ values (0.08 for MC-Glauber and 0.16 for MC-KLN initial conditions) are slightly too small [but not by much, as seen by the fact that increasing $(\eta/s)_{\rm QGP}$ by 0.08 leads to a strong underprediction of all data sets], and that the slightly larger values of 0.10 for MC-Glauber and 0.20 for MC-KLN extracted in [1] from fluctuation-corrected v_2 data would give better agreement here, too. Figure 6(b) shows that with reaction-plane averaged initial conditions the VISHNU results agree very well with the $v_2\{4\}$ data, supporting the argument [39,40] that $\langle\varepsilon_{\rm RP}\rangle \approx \varepsilon_{\rm s}$ provides a good substitute for $\varepsilon_{\rm part}\{4\}$. Again, using the slightly larger $(\eta/s)_{\rm QGP}$ values from [1] would further improve the agreement.

We note the inability of VISHNU to describe the elliptic flow in the most peripheral collisions where the

experimentally measured values remain large, whereas the theoretical predictions decrease rapidly with increasing impact parameter. This drop is related to the decreasing lifetime of the fireball (which is even shorter for runs with MC-KLN initial conditions than for Glauber profiles, due to the sharper edges of the MC-KLN profiles which lead to faster radial acceleration). Shorter lifetimes leave less time for generating elliptic flow in the fluid dynamic QGP stage, and the highly dissipative hadronic stage cannot compensate for this. Calculations with an ideal hydro + cascade model that use a different hadronic rescattering algorithm (JAM instead of UrQMD) appear to share this feature [42]. The fact that the $v_2\{4\}$ data do not show this decrease indicates that nonflow contributions (which are not included in the model) are not to blame. We do not know how to obtain larger v_2 values from the model at large impact parameters.

V. SUMMARY AND CONCLUSIONS

We have utilized the recently developed hybrid code VISHNU, which couples a relativistic viscous fluid dynamical description of the quark-gluon plasma (QGP) with a microscopic Boltzmann cascade for the late hadronic rescattering stage, to calculate charged and identified hadron spectra and elliptic flow measured in 200 A GeV Au + Au collisions at the Relativistic Heavy-Ion Collider (RHIC). We find that, after suitable readjustments of initial conditions, the p_T spectra of identified hadrons (pions and protons) are rather insensitive to the choice of the value of the specific shear viscosity η/s, whereas the eccentricity-scaled elliptic flow v_2/ε shows strong sensitivity to η/s. Using initial conditions that incorporate event-by-event fluctuations in the initial shape and orientation of the collision fireball and values $(\eta/s)_{\rm QGP}$ for the specific shear viscosity of the quark-gluon plasma that were recently extracted from the measured centrality dependence of the eccentricity-scaled, p_T-integrated charged hadron elliptic flow $v_{2,\rm ch}/\varepsilon$ [1], we were able to obtain universally good agreement between theory and experiment for the p_T spectra and differential elliptic flow $v_2(p_T)$ for both pions and protons at all collision centralities. Our analysis validates the constraints on η/s reported in our previous work, namely that the QGP shear viscosity for $T_{\rm c} < T \lesssim 2T_{\rm c}$ lies within the range $1 < 4\pi(\eta/s)_{\rm QGP} < 2.5$, with the remaining uncertainty dominated by insufficient theoretical control over the initial source eccentricity ε.

ACKNOWLEDGMENTS

We gratefully acknowledge fruitful discussions with P. Huovinen, H. Masui, A. Poskanzer, S. Voloshin, and A. Tang. We specifically thank A. Poskanzer for computing for us the α values listed in Table I and R. Snellings for providing some of the data shown in Fig. 6. This work was supported by the US Department of Energy under Grants No. DE-AC02-05CH11231, No. DE-FG02-05ER41367, No. DE-SC0004286, and (within the framework of the JET Collaboration) No. DE-SC0004104. T.H. acknowledges support through Grant-in-Aid for Scientific Research No. 22740151 and through the Excellent Young Researchers Oversea Visit Program (No. 213383) of the Japan Society for the Promotion of Science. We gratefully acknowledge extensive computing resources provided to us by the Ohio Supercomputer Center.

APPENDIX

In this Appendix we add a few aspects that, due to space limitations, were left out from the discussion in Ref. [1] of the almost universal dependence of the eccentricity-scaled elliptic flow v_2/ε on the charged hadron multiplicity density $(1/S)dN_{\rm ch}/dy$ on which our extraction of the QGP shear viscosity $(\eta/s)_{\rm QGP}$ from RHIC data was based. Specifically, we show that the universality of this dependence [i.e., the feature that it only depends on $(\eta/s)_{\rm QGP}$ but not on any details of the initial conditions for the hydrodynamic evolution which affect the initial eccentricity ε and transverse area S of the expanding fireball] holds not only for the participant-plane averaged fluctuating initial profiles used in [1] but also for the reaction-plane averaged profiles used here in Fig. 6(b). Furthermore, it is insensitive to the smearing area σ_s used in the MC-Glauber model of Ref. [10] that describes the width of the transverse distribution of matter created in each nucleon-nucleon collision. However, the source eccentricity ε itself depends on this smearing area, and hence the $(\eta/s)_{\rm QGP}$ value extracted by comparing the universal theoretical v_2/ε vs $(1/S)dN_{\rm ch}/dy$ curves for different η/s with a given set of experimental v_2 vs $dN_{\rm ch}/dy$ data also depends on this parameter.

In the traditional MC-Glauber model, one samples the positions of nucleons according to the nuclear density distributions of the two colliding nuclei and calculates the participant eccentricity from the transverse positions of the wounded nucleons and/or binary collision points, described by δ functions in the transverse plane. Hirano and Nara [10] pointed out that, since the measured nuclear density distribution represents a folding of the distribution of nucleon centers with the finite size of each nucleon, the nuclear distribution used for sampling the positions of the nucleon centers must be described by different Woods-Saxon parameters than the measured nuclear density. Following Ref. [10], we therefore use for the distribution of nucleon centers in a Au nucleus a Woods-Saxon distribution with radius $R_{\rm Au} = 6.42$ fm and surface thickness $d_{\rm Au} = 0.44$ fm (instead of the frequently used parameters $R_{\rm Au}^{\rm meas.} = 6.38$ fm and $d_{\rm Au}^{\rm meas.} = 0.535$ fm that describe the measured nuclear density distribution of Au). We then distribute the entropy of particles emitted by a wounded nucleon or created in a binary nucleon-nucleon collision homogeneously in a cylinder of radius $r_s = \sqrt{\sigma_s/\pi}$ (where σ_s is the so-called "transverse smearing area"), centered at the position of the wounded nucleon or the collision point and aligned with the beam direction. (The same procedure was used in Ref. [22] without, however, first correcting the Woods-Saxon parameters of the distribution of nucleon centers for the finite nucleon size.)

The value of the smearing area σ_s is not known *a priori* since it depends on unknown aspects of prethermal decoherence and entropy production processes. Theoretically, it is limited from

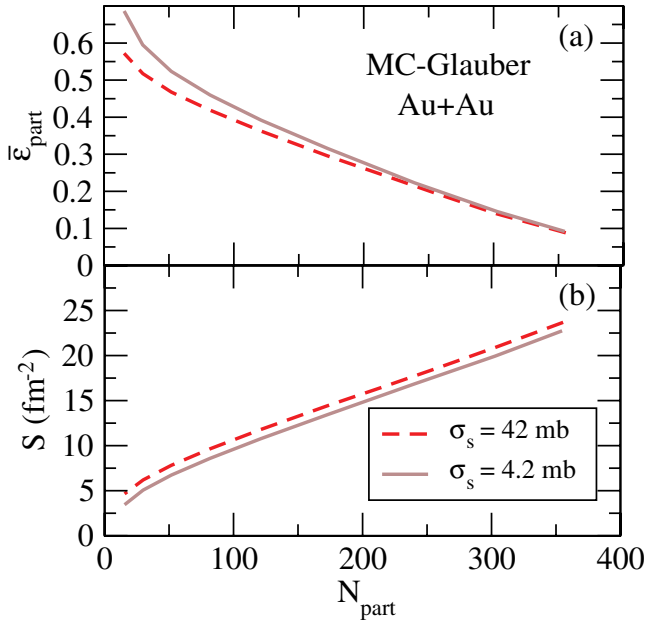

FIG. 7. (Color online) Eccentricity $\bar{\varepsilon}_{\rm part}$ (a) and transverse area S (b) of the participant-plane averaged initial entropy density distribution from the MC-Glauber model, for smearing areas $\sigma_s = 42$ and 4.2 mb, respectively. (See also Fig. 4 in Ref. [22] for comparison.)

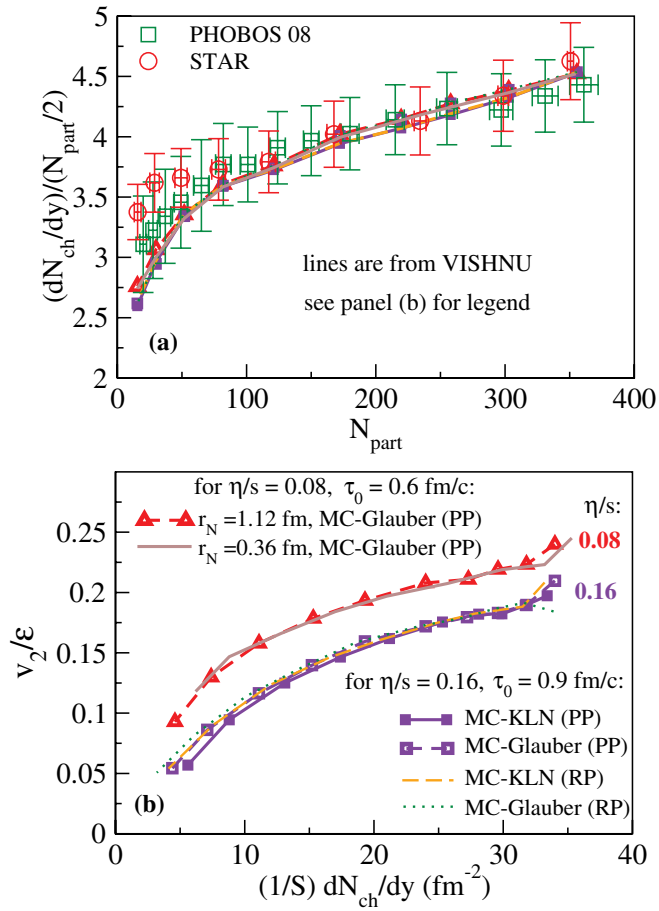

FIG. 8. (Color online) (a) Centrality dependence of the charged hadron rapidity density per participant pair $(dN_{\rm ch}/dy)/(N_{\rm part}/2)$. Experimental data are from STAR [17] and PHOBOS [45], using $dN_{\rm ch}/dy = 1.16\, dN_{\rm ch}/d\eta$ for the PHOBOS data. Theoretical lines are explained in the text. (b) Eccentricity-scaled elliptic flow v_2/ε as function of multiplicity density $(1/S)(dN_{\rm ch}/dy)$, for different values of $(\eta/s)_{\rm QGP}$, using participant-plane (PP) and reaction-plane (RP) averaged initial entropy density profiles from the MC-KLN and MC-Glauber models, normalized to $(dN_{\rm ch}/dy)_{\rm max} = 810$ in the most central (0%–5%) Au + Au collisions. Insensitivity to the smearing area σ_s in the MC-Glauber models is also shown.

below by the uncertainty principle which does not permit localization of the production points of secondary particles with average transverse momentum $\langle p_T \rangle$ to an average distance $r_s < 1/\langle p_T \rangle$ from the classical collision point. We explore the choices $\sigma_s = 42$ mb [10,22] and 4.2 mb. The smaller value is an approximation to pointlike secondary particle production (our code for calculating the participant-plane averaged initial density requires a nonvanishing σ_s); theoretically it is disfavored by the above uncertainty argument.

Figure 7 shows the eccentricity (a) and transverse area (b) of the participant-plane averaged initial entropy density distribution as a function of the number $N_{\rm part}$ of participant ("wounded") nucleons in Au + Au collisions, for two values of the smearing area σ_s. We see that a smaller smearing area (more pointlike particle production) leads to larger initial fireball eccentricities $\varepsilon_{\rm part}$ and smaller transverse areas S. While the effect of varying σ_s on S is simply an offset, for $\varepsilon_{\rm part}$ it leads to a change in the slope of its centrality dependence: changing σ_s affects $\varepsilon_{\rm part}$ more strongly in peripheral collisions (where the nuclear overlap region is small and strongly deformed) than in central ones [22].

Figure 8 illustrates that changing the smearing area in the MC-Glauber model has no effect on the centrality dependence of the produced charged hadron multiplicity (a) nor on the universality of v_2/ε vs $(1/S)dN_{\rm ch}/dy$ (b). In Fig. 8(b) one sees [see solid brown line without symbols for $(\eta/s)_{\rm QGP} = 0.08$] that, for smaller $\sigma_s = 4.2$ mb, the reduced fireball area shown in Fig. 7(b) shifts the entire curve toward the right. The shift is, however, not horizontal but rather diagonal such that, where they overlap, the shifted curve lies on top of the line for the larger value $\sigma_s = 42$ mb. The upward component of the shift of the $\sigma_s = 4.2$ mb line arises from an increased QGP lifetime, due to the larger initial entropy density resulting from the smaller initial area S; a longer QGP lifetime in turn results in a larger momentum anisotropy at the beginning of the hadronic stage, since at RHIC energies the QGP never lives long enough for the fireball eccentricity to completely decay before hadronization. Larger momentum anisotropy at the beginning of the hadronic rescattering stage leads to more elliptic flow for the finally emitted hadrons.

In Fig. 8 we also show curves obtained from VISHNU using reaction-plane averaged (RP) initial profiles instead of participant-plane averaged (PP) ones. One sees that the centrality dependence of the final charged multiplicity per participant [Fig. 8(a)] and the dependence of v_2/ε on the multiplicity density $(1/S)dN_{\rm ch}/dy$ are insensitive to how we average the fluctuating initial profiles from the MC-KLN and MC-Glauber models when constructing the smooth initial entropy density

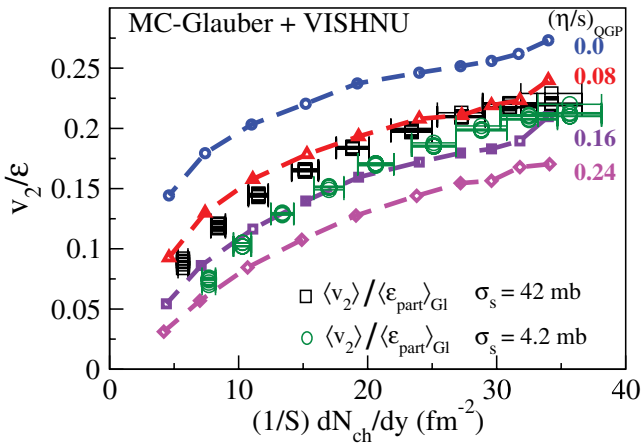

FIG. 9. (Color online) Comparison of the universal theoretical curves for $v_2[\eta/s]/\varepsilon$ vs $(1/S)(dN_{ch}/dy)$ from the MC-Glauber model with $\sigma_s = 42$ mb [1] with experimental data for $\langle v_2\rangle$ [21], normalized by the eccentricity $\langle\varepsilon_{part}\rangle$ and transverse fireball area S of the initial profile from the participant-plane averaged MC-Glauber model with standard ($\sigma_s = 42$ mb) and reduced ($\sigma_s = 4.2$ mb) smearing areas.

profile for the hydrodynamic evolution. Due to numerical cost we here show only curves for shear viscosity $(\eta/s)_{QGP} = 0.16$ for both MC-Glauber and MC-KLN models. We have made spot checks to convince ourselves that the scaling shown in Fig. 8 also works for other choices of $(\eta/s)_{QGP}$.

Figure 9 is a modified version of Fig. 2(b) in [1] which was used to extract the preferred value of $(\eta/s)_{QGP}$ from experimental data by comparing them with VISHNU calculations using participant-plane averaged initial conditions from the MC-Glauber model. We remind the reader that, even though theoretically the dependence of v_2/ε on $(1/S)dN_{ch}/dy$ is universal (at least at a fixed collision energy [14]) and depends only on a single parameter $(\eta/s)_{QGP}$, but not on the initial profile, we do not know the correct initial profile that drives the generation of elliptic flow in the actual experiments. Since different initial conditions have different eccentricities, the same set of experimental v_2 and dN_{ch}/dy data yields different v_2/ε and $(1/S)dN_{ch}/dy$ when normalized by ε and S from different initial state models, resulting in different extracted values for $(\eta/s)_{QGP}$ from a comparison with the universal theory curves. The larger eccentricities and smaller overlap areas resulting from a MC-Glauber initialization with reduced smearing area $\sigma_s = 4.2$ mb lead to smaller v_2/ε and larger $(1/S)dN_{ch}/dy$ values (green circled data in Fig. 9) than for the MC-Glauber model with standard smearing ($\sigma_s = 42$ mb, black squares). This results in a larger preferred value $(\eta/s)_{QGP}$ (closer to 0.16 than the value of 0.08 we obtained when postulating MC-Glauber initial conditions with standard smearing). Furthermore, normalization of the experimental data with MC-Glauber (ε, S) values for reduced smearing changes the slope of the dependence of v_2/ε on $(1/S)dN_{ch}/dy$, and it no longer agrees with the slope of the universal theoretical curves. We conclude that the comparison of experimental data with VISHNU results disfavors the hypothesis that the experimentally measured elliptic flow is generated by initial conditions that can be described by a MC-Glauber model with almost pointlike secondary particle production. This conclusion aligns nicely with the theoretical prejudice against such a model on the basis that it would violate the uncertainty principle, as discussed above.

[1] H. Song, S. A. Bass, U. Heinz, T. Hirano, and C. Shen, Phys. Rev. Lett. **106**, 192301 (2011).

[2] H. Song, S. A. Bass, and U. Heinz, Phys. Rev. C **83**, 024912 (2011).

[3] S. A. Bass *et al.*, Prog. Part. Nucl. Phys. **41**, 255 (1998).

[4] H. Song and U. Heinz, Phys. Lett. B **658**, 279 (2008); Phys. Rev. C **77**, 064901 (2008); **78**, 024902 (2008).

[5] C. Shen, U. Heinz, P. Huovinen, and H. Song, Phys. Rev. C **82**, 054904 (2010).

[6] L. P. Csernai, J. I. Kapusta, and L. D. McLerran, Phys. Rev. Lett. **97**, 152303 (2006).

[7] P. Braun-Munzinger, D. Magestro, K. Redlich, and J. Stachel, Phys. Lett. B **518**, 41 (2001).

[8] P. Romatschke and U. Romatschke, Phys. Rev. Lett. **99**, 172301 (2007); M. Luzum and P. Romatschke, Phys. Rev. C **78**, 034915 (2008).

[9] M. L. Miller, K. Reygers, S. J. Sanders, and P. Steinberg, Annu. Rev. Nucl. Part. Sci. **57**, 205 (2007).

[10] T. Hirano and Y. Nara, Phys. Rev. C **79**, 064904 (2009); Nucl. Phys. A **830**, 191c (2009).

[11] H. J. Drescher and Y. Nara, Phys. Rev. C **75**, 034905 (2007); **76**, 041903(R) (2007).

[12] D. Kharzeev and M. Nardi, Phys. Lett. B **507**, 121 (2001); D. Kharzeev and E. Levin, *ibid.* **523**, 79 (2001); D. Kharzeev, E. Levin, and M. Nardi, Phys. Rev. C **71**, 054903 (2005); Nucl. Phys. A **730**, 448 (2004); **743**, 329(E) (2004).

[13] M. Miller and R. Snellings, arXiv:nucl-ex/0312008; B. Alver *et al.*, Phys. Rev. Lett. **104**, 142301 (2010).

[14] T. Hirano, P. Huovinen, and Y. Nara, Phys. Rev. C **83**, 021902 (2011).

[15] J. Adams *et al.* (STAR Collaboration), Phys. Rev. Lett. **92**, 112301 (2004); B. I. Abelev *et al.* (STAR Collaboration), *ibid.* **97**, 152301 (2006).

[16] The data shown in [15] are available in tabular form at [http://drupal.star.bnl.gov/STAR/files/starpublications/65/data.html].

[17] B. I. Abelev *et al.* (STAR Collaboration), Phys. Rev. C **79**, 034909 (2009).

[18] S. S. Adler *et al.* (PHENIX Collaboration), Phys. Rev. C **69**, 034909 (2004).

[19] J. Adams *et al.* (STAR Collaboration), Phys. Rev. C **72**, 014904 (2005).

[20] S. A. Voloshin, A. M. Poskanzer, and R. Snellings, in *Relativistic Heavy Ion Physics*, Landolt-Börnstein New Series, Vol. I/23, edited by R. Stock (Springer Verlag, New York, 2010), Chap. 5, arXiv:0809.2949 [nucl-ex]

[21] J. Y. Ollitrault, A. M. Poskanzer, and S. A. Voloshin, Phys. Rev. C **80**, 014904 (2009).

[22] B. Alver *et al.*, Phys. Rev. C **77**, 014906 (2008).

[23] B. H. Alver, C. Gombeaud, M. Luzum, and J. Y. Ollitrault, Phys. Rev. C **82**, 034913 (2010).

[24] Z. Qiu and U. Heinz, arXiv:1104.0650 [nucl-th].

[25] A. Adare *et al.* (PHENIX Collaboration), Phys. Rev. Lett. **105**, 062301 (2010).
[26] Talks presented by A. Taranenko at the joint CATHIE/TECHQM Workshop, Brookhaven National Laboratory, Dec. 14–18, 2009, and by R. A. Lacey at the INT program Quantifying the Properties of Hot QCD Matter, Institute for Nuclear Theory, May 24–July 16, 2010.
[27] R. Lacey and P. Sorensen (private communication).
[28] A. M. Poskanzer (private communication).
[29] J. Y. Ollitrault, Phys. Rev. D **46**, 229 (1992).
[30] U. Heinz, arXiv:nucl-th/0512051.
[31] D. A. Teaney, in *Quark-Gluon Plasma 4*, edited by R. C. Hwa and X.-N. Wang (World Scientific, Singapore, 2010), p. 207; arXiv:0905.2433.
[32] T. Hirano and M. Gyulassy, Nucl. Phys. A **769**, 71 (2006).
[33] D. Teaney, Phys. Rev. C **68**, 034913 (2003).
[34] K. Dusling and D. Teaney, Phys. Rev. C **77**, 034905 (2008).
[35] A. Monnai and T. Hirano, Phys. Rev. C **80**, 054906 (2009).
[36] H. Song and U. Heinz, Phys. Rev. C **81**, 024905 (2010).
[37] R. P. G. Andrade, F. Grassi, Y. Hama, T. Kodama, and W. L. Qian, Phys. Rev. Lett. **101**, 112301 (2008); H. Petersen and M. Bleicher, Phys. Rev. C **79**, 054904 (2009); K. Werner, I. Karpenko, T. Pierog, M. Bleicher, and K. Mikhailov, *ibid.* **82**, 044904 (2010); H. Holopainen, H. Niemi, and K. J. Eskola, *ibid.* **83**, 034901 (2011); B. Schenke, S. Jeon, and C. Gale, Phys. Rev. Lett. **106**, 042301 (2011).
[38] G. Y. Qin, H. Petersen, S. A. Bass, and B. Müller, Phys. Rev. C **82**, 064903 (2010).
[39] R. S. Bhalerao and J. Y. Ollitrault, Phys. Lett. B **641**, 260 (2006).
[40] S. A. Voloshin, A. M. Poskanzer, A. Tang, and G. Wang, Phys. Lett. B **659**, 537 (2008).
[41] S. Voloshin and Y. Zhang, Z. Phys. C **70**, 665 (1996).
[42] T. Hirano, P. Huovinen, and Y. Nara, arXiv:1012.3955 [nucl-th].
[43] K. Aamodt *et al.* (ALICE Collaboration), Phys. Rev. Lett. **105**, 252302 (2010).
[44] S. Afanasiev *et al.* (PHENIX Collaboration), Phys. Rev. C **80**, 024909 (2009).
[45] B. B. Back *et al.*, Phys. Rev. C **70**, 021902 (2004); B. Alver *et al.*, *ibid.* **80**, 011901 (2009).